BIOMOLECULES & THERAPEUTICS

Original Article
Biomol Ther 29(5), 506-518 (2021)

Novel Anti-Angiogenic and Anti-Tumour Activities of the N-Terminal Domain of NOEY2 via Binding to VEGFR-2 in Ovarian Cancer

Seung Bae Rho[1], Keun Woo Lee[2], Seung-Hoon Lee[3], Hyun Jung Byun[4], Boh-Ram Kim[1,4,*] and Chang Hoon Lee[4,*]

[1]Division of Translational Science, Research Institute, National Cancer Center, Goyang 10408,
[2]Department of Biochemistry, Division of Applied Life Science, Environmental Biotechnology National Core Research Center, Gyeongsang National University, Jinju 52828,
[3]Department of Life Science, Yong In University, Yongin 17092,
[4]BK21 FOUR Team and Integrated Research Institute for Drug Development, College of Pharmacy, Dongguk University, Seoul 10326, Republic of Korea

Abstract

The imprinted tumour suppressor NOEY2 is downregulated in various cancer types, including ovarian cancers. Recent data suggest that NOEY2 plays an essential role in regulating the cell cycle, angiogenesis and autophagy in tumorigenesis. However, its detailed molecular function and mechanisms in ovarian tumours remain unclear. In this report, we initially demonstrated the inhibitory effect of NOEY2 on tumour growth by utilising a xenograft tumour model. NOEY2 attenuated the cell growth approximately fourfold and significantly reduced tumour vascularity. NOEY2 inhibited the phosphorylation of the signalling components downstream of phosphatidylinositol-3'-kinase (PI3K), including phosphoinositide-dependent protein kinase 1 (PDK-1), tuberous sclerosis complex 2 (TSC-2) and p70 ribosomal protein S6 kinase (p70S6K), during ovarian tumour progression via direct binding to vascular endothelial growth factor receptor-2 (VEGFR-2). Particularly, the N-terminal domain of NOEY2 (NOEY2-N) had a potent anti-angiogenic activity and dramatically downregulated VEGF and hypoxia-inducible factor-1α (HIF-1α), key regulators of angiogenesis. Since no X-ray or nuclear magnetic resonance structures is available for NOEY2, we constructed the three-dimensional structure of this protein via molecular modelling methods, such as homology modelling and molecular dynamic simulations. Thereby, Lys15 and Arg16 appeared as key residues in the N-terminal domain. We also found that NOEY2-N acts as a potent inhibitor of tumorigenesis and angiogenesis. These findings provide convincing evidence that NOEY2-N regulates endothelial cell function and angiogenesis by interrupting the VEGFR-2/PDK-1/GSK-3β signal transduction and thus strongly suggest that NOEY2-N might serve as a novel anti-tumour and anti-angiogenic agent against many diseases, including ovarian cancer.

Key Words: Ovarian cancer, VEGFR-2, NOEY2 N-terminal, Antiangiogenic activity, Homology modelling, Tumour suppressor

INTRODUCTION

Angiogenesis, which is the sprouting of new blood vessels from pre-existing vasculature, is a crucial process in tumour pathogenesis and invasive tumour growth as well as development, wound repair and reproduction (Risau, 1997). Thus, anti-angiogenesis-based therapies are useful modalities for the treatment of cancer. Angiogenesis is essential for the growth and progression of tumours because it enables the delivery of oxygen and nutrients to the growing tumour (Li *et al*., 2018; Lugano *et al*., 2020). Vascular endothelial growth factor (VEGF) and hypoxia-inducible factor-1α (HIF-1α) play pivotal roles in tumour angiogenesis. One of the key mediators of blood-vessel formation during development is VEGF, promoting the proliferation, survival, and migration of endothelial cells (Ferrara, 2002). Receptors called vascular endothelial growth factor receptor-1 (VEGFR-1; Flt-1), VEGFR-2 (KDR/Flk-1), and VEGFR-3 (Flt-4) regulate pathological and physiological angiogeneses. Interestingly, VEGFR-1 is also a key receptor in developmental angiogenesis and does not appear to be an

Open Access **https://doi.org/10.4062/biomolther.2021.121**

Received Jul 19, 2021 **Revised** Jul 30, 2021 **Accepted** Aug 3, 2021
Published Online Sep 1, 2021

***Corresponding Authors**
E-mail: qtrami@gmail.com (Kim BR), uatheone@dongguk.edu (Lee CH)
Tel: +82-31-961-5434 (Kim BR), +82-31-961-5213 (Lee CH)
Fax: +82-31-961-5206 (Kim BR), +82-31-961-5206 (Lee CH)

essential factor for pathogenic angiogenesis (Hicklin and Ellis, 2005). By contrast, VEGFR-2 possesses potent tyrosine kinase activity and is the main signal transducer for cellular events involved in tumour angiogenesis and tumour formation, including cell proliferation, migration, invasion, metastasis and survival (Spannuth *et al*., 2009; Wang *et al*., 2020).

VEGF is activated under hypoxic conditions via the oxygen-sensing factor HIF-1α. HIF-1 is a heterodimer consisting of HIF-1α and HIF-1β subunits and is an important transcription factor that mediates new blood vessel formation by regulating the expression of the angiogenic factor VEGF. Additionally, HIF-1 plays a major role in cellular responses to hypoxia in healthy and carcinoma cells (Masoud and Li, 2015). Hypoxia plays a pivotal role in tumour development, progression of vascular-related diseases and subsequent pathological angiogenesis involving upregulation of VEGF and VEGF-related target molecules. HIF-1α is a well-validated therapeutic target protein found in many solid tumours. It is the main regulator of several factors pivotal for tumour angiogenesis, involving those that modulate tumour progression, embryonic development, cell metabolism, apoptotic cell death, and metastasis (Wigerup *et al*., 2016; Jing *et al*., 2019). HIF-1α is over-expressed in various human cancers, including brain, cervical, ovarian, gastric, bladder, breast, and pancreatic cancers. In addition, its cellular activity influences both tumour angiogenesis and tumourigenicity (Rankin and Giaccia, 2008).

NOEY2, a small GTP-binding protein belonging to the Ras superfamily, shares 60% homology with Ras and Rap (Gasper *et al*., 2010). NOEY2 can exist in a GTP-bound form and has various binding partners. NOEY2 harbours a unique sequence of 34 amino acids at its N-terminus (NOEY2-N), which is not often seen in other members of the Ras family (Luo *et al*., 2003). NOEY2 is expressed in healthy breast and ovarian epithelial cells, but its expression is either lost or down-regulated in breast and ovarian cancers. NOEY2 can shorten signalling via Ras/mitogen-activated protein kinase (MAPK), activates c-Jun N-terminal kinase, induces $p21^{WAF1/CIP1}$, down-regulates cyclin D1, and can also trigger apoptosis (Bao *et al*., 2002). NOEY2 is a unique tumour suppressor gene of the Ras superfamily, unlike other members of the Ras superfamily of proto-oncogenes (Yu *et al*., 1999). Although the molecular mechanisms whereby NOEY2 inhibits cell proliferation and motility are still vague, the N-terminus, which differentiates NOEY2 from other Ras proteins, seems vital for the tumour suppressor activity of NOEY2 (Nishimoto *et al*., 2005).

In this study, we confirmed the anti-tumour and anti-angiogenic effects of NOEY2 in a mouse model of ovarian cancer. We also validated the anti-tumour and anti-angiogenic effects of NOEY2-N *in vitro* by using human umbilical vein endothelial cells (HUVECs) and ovarian carcinoma cells. Next, we established a molecular model via homology modelling and molecular dynamic simulations, whereby potential key residues in NOEY2-N were identified. We expect that our findings will facilitate the discovery of anticancer drugs targeting Ras- family oncogenes.

MATERIALS AND METHODS

Cell culture conditions, animals and antibodies

Human ovarian carcinoma cell lines (SKOV-3 and OVCAR-3) and human embryonic kidney 293T (HEK293T) cells were maintained in accordance with American Type Culture Collection (ATCC, Manassas, VA, USA) instructions. HUVECs were obtained from Clonetics (Walkersville, MD, USA), and were grown in EGM-2 BulletKit medium (Clonetics) on 0.3% gelatin (Sigma, St. Louis, MO, USA) coated dishes. Cells were seeded in a humidity chamber at 37°C with 5% carbon dioxide. Specific pathogen-free BALB/c-nu/nu mice (approximately 5-6 weeks old) were supplied by Orientbio (Seongnam, Korea). All animal studies were approved by the Institutional Animal Care and Use Committee (IACUC) at the Research Institute of the National Cancer Center (Goyang, Korea). The primary antibodies used were anti-caspase-3, anti-Bcl-2 anti-Bcl-xL, anti-Bax, anti-p53, anti-VEGFR-1, anti-VEGFR-2, anti-phospho-VEGFR-2 (Tyr-951), anti-phospho-VEGFR-2 (Tyr-1175), anti-HIF-1α, anti-survivin, anti-COX-2, anti-PI3K, anti-phospho-PI3K, anti-PDK-1, anti-phospho-PDK-1 (Ser241), anti-Akt, anti-phospho-Akt (Ser473 and Thr308), anti-mTOR, anti-phospho-mTOR (Ser2448), anti-TSC2, anti-phospho-TSC2 (Ser1462), anti-p70S6K, anti-phospho-p70S6K (Thr421) (Cell Signaling, Beverly, MA, USA), anti-p27, anti-p21, anti-VEGF, anti-Ki67, anti-CD31 (PECAM-1) (Ab-1; Oncogene, Cambridge, MA, USA), anti-PARP, anti-XIAP (BD Biosciences, San Jose, CA, USA), anti-cyclin D1, anti-CDK4, anti-NF-κB, anti-GSK-3β, anti-phospho-GSK-3β (Ser-9) (Santa Cruz Biotechnology, Santa Cruz, CA, USA), anti-PCNA (Dako Denmark A/S, Glostrup, Denmark), anti-NOEY2 (BD Pharmingen, San Diego, CA, USA), and anti-NOEY2 and anti-β-actin (Sigma).

Conduction of NOEY2 overexpressing vector and transfection

The full length of NOEY2 was amplified by PCR and cloned into the *EcoRI* and *XhoI* fragment of the pcDNA3.1 expression vector. The primers of NOEY2 were designed as follows: forward, 5'-ATTGAATTCATGGGTAACGCCAGCTTTGGC-3'; reverse, 5'-CGGCTCGAGTCACATGATTATGCACTTGTC-3'. Subsequently, the plasmid pcDNA3.1-NOEY2 was transfected into SKOV-3 cells using Lipofectamine 2000 reagent (Invitrogen, Carlsbad, CA, USA), strictly following the manufacturer's instructions. The non-transfected control cells and the empty vector transfected (pcDNA3.1 only) cells were evaluated in parallel as a control. The stably transfected cells were selected by G418 (1 mg/mL, Invitrogen) after 10-14 days of two days post-transfection.

Xenograft mouse model and immunohistochemistry

In brief, human SKOV-3 ovarian carcinoma cells (2.3×10^6), stably transfected with NOEY2 or empty vector, were injected subcutaneously into 5- to 6-week-old BALB/c-nu/nu mice and allowed to form tumours 70-100 mm^3 in size. Tumour volume was calculated in three dimensions using callipers and evaluated by the following formula: tumour volume (mm^3)=($a\times b^2$)/2, where a=length in mm and b=width in mm. Bodyweight was assessed every other day. Tumours were then excised and weighed, and half were frozen. Half were fixed in 10% neutral-buffered formalin (NBF) to generate paraffin blocks for sectioning, haematoxylin and eosin (H&E) staining and immunohistochemistry.

For immunohistochemistry, tumour samples from xenografted mice were collected, fixed and serially sectioned as previously reported (Yu *et al*., 2021). Slides were then incubated with an anti-mouse CD31 (platelet-derived endothelial cell adhesion molecule; PECAM-1) (Abcam, Cambridge, UK)

overnight at 4°C, followed by a streptavidin-peroxidase complex for 1 h at room temperature. Microvessel density was quantified in five randomly selected individual tumour fields (at 40× magnification) from each sample. The number of microvessels was also counted under a high-power microscope (at 400× magnification). Additional slides were stained with H&E (Sigma) according to the supplier's instructions. All immunochemical analyses were performed using an Axiophot 2 apparatus (Carl Zeiss MicroImaging Inc., Thornwood, NY, USA).

For western blotting analysis, protein lysates were prepared from homogenised frozen tumour tissues, and a Bradford protein assay was used to determine protein concentration. Equal amounts of protein (20 μg) were loaded onto 8-12% SDS-PAGE.

Flow cytometric analysis for apoptotic cell death and cell proliferation assay

For analysis of the DNA content using flow cytometry, SKOV-3 and OVCAR-3 cancer cells were grown at a density of approximately 3.5-4.0×10^5 in 60-mm plates. Cells were detached using trypsin and rinsed twice with phosphate-buffered saline (PBS). The pellets were re-suspended with binding buffer and incubated with fluorescein isothiocyanate (FITC)-labelled annexin V and propidium iodide (PI) for 15 min according to the supplier's instructions (BD Pharmingen, Mississauga, ON, Canada). The labelled cells were analysed using a fluorescence activated cell sorting (FACS) Vantage BD FACSCalibur flow cytometer (Becton-Dickinson, Franklin Lakes, NJ, USA). Cell viability was measured using the CellTiter-Glo luminescent assay kit (Promega, Madison, WI, USA) according to the manufacturer's instructions. In brief, cells were maintained at a density of 4.0×10^3 per well in 96-well plates. After 24 h, cells were transfected/treated with control (empty-inserted vector only), NOEY2(wt), or three truncated mutants, respectively. Cell viability was calculated using CellTiter-Glo reagent (Promega, Madison, WI, USA).

Caspase-3 activity assay

For caspase-3 activity, cells (2.4×10^6) were maintained in either the absence or presence of NOEY2 for 24 h at 37°C. Caspase-3 activity was calculated using actyl-DEVD-7-amino-4-trifluoromethyl coumarin as the substrate, according to the supplier's instructions (BD Pharmingen). In brief, the cells were placed with VP-16 (100 μg/mL) for 24 h, lysed in lysis buffer, and centrifuged at 4°C for 25 min at 12,000 *g*. The activity was measured in the supernatant fraction according to proteolytic cleavage of the colourimetric substrate using a Spectramax 340 microplate reader (Molecular Devices, San Jose, CA, USA) in fluorescence mode with excitation at 405 nm and emission at 505 nm (Kang *et al*., 2012). For analysis of poly (ADP-ribose) polymerase (PARP) cleavage, we performed the protocols as described in the previous study (Maharjan *et al*., 2019). Briefly, 50 μg of protein was incubated with 60 μM biotinylated nicotinamide adenine dinucleotide in a 50 μL final volume of PARP reaction buffer (50 mM Tris-HCl, pH 8.0 and 25 mM magnesium chloride) for 1 h at 37°C. The reaction was stopped by adding sodium dodecyl sulphate (SDS) loading-dye buffer, and the products were separated using SDS-polyacrylamide gel electrophoresis (PAGE) and autoradiography.

Yeast two-hybrid (Y2H) protein analysis

For bait construction with human NOEY2, cDNA encoding full-length human NOEY2 was cloned into the *Eco*RI and *Xho*I restriction enzyme sites of the pGilda/LexA yeast shuttle vector. The bait pGilda/LexA-NOEY2-N plasmid was transformed into a yeast strain EGY48 using a modified lithium acetate protocol (Rho *et al*., 1999). Human VEGFR-1 and VEGFR-2 were inserted, with each cDNA encoding a full-length into multi-cloning sites (MCS) of the pJG4-5 plasmid vector, which included B42 fusion proteins (Clontech, Palo Alto, CA, USA). VEGFR-1 or VEGFR-2 cDNAs encoding pJG4-5 fusion proteins were introduced into yeast-competent cells that already contained pGilda/LexA-NOEY2-N. At the same times, the transformants were selected based on their tryptophan prototrophy (plasmid marker) on a synthetic medium (Ura, His, Trp) containing 2% w/v glucose. The binding activity of the interaction was calculated according to the previously described methods (Rho *et al*., 1996).

Co-immunoprecipitation (Co-IP) and western blotting

Co-IP was carried out as described previously (Rho *et al*., 2020). Briefly, cells were trypsinised and then centrifuged. Cell pellets were washed in cold PBS and re-suspended in lysis buffer supplemented with protease inhibitors. The cell lysates were incubated with an anti-Flag antibody (Santa Cruz Biotechnology) and then precipitated with protein A-agarose (Rho *et al*., 1999). About 20-30 μg of precipitated proteins were separated by 10-12% SDS-PAGE and transferred to Immobilon P membrane (Millipore Corporation, Billerica, MA, USA). After blocking, the membranes were incubated with the indicated specific primary antibodies, including anti-NOEY2 and anti-VEGFR-2. The membranes were rinsed three times in Tris-buffered saline, and Tween 20 washing buffer for 5 min, and then horseradish peroxidase-conjugated secondary antibodies were incubated for 1 h at room temperature. The blots were visualised using an enhanced chemiluminescence detection system (GE Healthcare, Piscataway, NJ, USA).

Luciferase reporter-gene analysis

The VEGFR-2 promoter fragment was cloned from human placental complementary DNA (cDNA) to evaluate VEGFR-2 promoter activity by PCR using primers: 5′-TAGCGAGCTCTGCCACAAGAAGTCCACACA-3′ (sense); 5′-CACCCGACCTGTCTGCCTTCC-3′ (antisense). The domain including the VEGFR-2 promoter (from −887 to +295) region was introduced between the *Sac*I and *Xho*I cloning sites of the pGL3 luciferase reporter expression vector (Promega). *In vitro*, VEGFR-2 promoter activity was performed as previously reported (Rho *et al*., 2012). Briefly, cells were transiently transfected with each indicated reporter plasmid. After lysis, cell extracts were incubated with the luciferase substrate reagent for 30 min at room temperature. Then, a 5 μL aliquot of each sample was placed into the MicroLumat Plus LB96V luminometer (Berthold Technologies, Bad Wildbad, Baden-Württemberg, Germany).

[^{3}H] Thymidine incorporation analysis

To measure endothelial cell proliferation, cells were seeded at a density of 3.0×10^4 per well of gelatinised plates in standard medium on day 0. Next, [^{3}H] thymidine incorporation analysis was carried out as reported previously (Kim *et al*., 2015).

NOEY2 three-dimensional structure generation using a molecular modelling method, homology modelling

For the main body, except for N-terminal 34 amino acids, three x-ray crystal structures from the Ras superfamily were used as a template structure: human Rap1A (Protein Data Bank code: 1GUA), Rap2A (3RAP) and H-Ras (1K8R) structures. However, for the N-terminal domain, only one NMR structure was available: human interleukin-6 (1IL6). For homology-modelling procedures, the MODELER module in the INSIGHT II program (Accelrys, Inc., San Diego, CA, USA) was used to manipulate sequence and structure and to perform the calculations.

Two-domain structure connection using MD simulations: computer-based native conformational search

All EM and MD calculations were performed with the DISCOVER module in the INSIGHT II program using the consistent-valence force-field (Dauber-Osguthorpe *et al*., 1988). A relatively small integration time step (1 fs) was used for the most exacting simulations. All the above MD simulations were done with distance-dependent dielectric constant and 12 Å of cut-off.

Endothelial cell tubular structure formation analysis

In vitro tube formation analysis was carried out as reported previously (Rho *et al*., 2020). HUVEC cells were seeded in Growth factor-reduced Matrigel (200 μL of 10 mg/mL; BD Biosciences) coated 24-well plate and then incubated for 48 h in M199 containing 1% FBS with/without 10 ng/mL VEGF. Morphological changes were photographed at 40× magnification. Capillary-like tubular structures were monitored using an inverted microscope equipped with a digital charge-coupled device camera (Zeiss, Oberkochen, Baden-Württemberg, Germany) and quantified using ImageLab imaging software (MCM Design, Copenhagen, Denmark).

Site-directed mutagenesis of human NOEY2

Pfu DNA polymerase (Stratagene, La Jolla, CA, USA) was employed according to the manufacturer's recommendations for all PCR amplifications. *Eco*RI and *Xho*I were used to cleave the resulting PCR product. The cleaved product was then cloned into pcDNA3.1 expression vector (Invitrogen). All point mutants of the *NOEY2* gene were obtained using the QuikChange (Stratagene) site-directed mutagenesis kit, according to the supplier's instructions. The sequences of the mutated residues were confirmed by automatic sequencing (ABI 373).

Statistical analysis

Data values presented as mean ± standard deviation (SD) and statistical comparisons were determined statistically using Student's *t*-test. A p-value of <0.05 was considered statistically significant.

RESULTS

NOEY2 is directly associated with the suppression of tumour growth and angiogenesis *in vivo*

To explore the direct anti-tumour and anti-angiogenic activities of NOEY2, we investigated the effects of NOEY2 on tumour growth in ovarian tumour xenografts *in vivo*. A stable SKOV-3 ovarian cancer cell line overexpressing NOEY2 was established as described in the Materials and Methods. Human SKOV-3 ovarian cancer cells, stably transfected with *NOEY2* or the empty vector, were subcutaneously injected into nude mice to induce the development of ovarian tumours. The tumour volume in the control group was notably increased after 14 days (mean volume 100 mm^3; Fig. 1A). However, the tumour growth in the NOEY2 group was approximately 70% less than in the control group (Fig. 1B). Subsequently, the tumour sections were stained with haematoxylin and eosin staining to observe the histological differences. The tumour sections from the control group revealed high-grade carcinoma with an irregular cell distribution and mitotic morphology (Fig. 1C). However, the tumours from the NOEY2 group had late-apoptotic or necrotic cells indicated with arrows (Fig. 1C). Additionally, the tissues from the NOEY2 and control group were stained for Ki67, a marker of cell proliferation. Ki67 expression was noticeably lower in the NOEY2 group versus the controls. Immunohistochemical findings for cleaved caspase-3 suggested an apoptotic effect of NOEY2 (Fig. 1C). To further clarify the cellular mechanisms underlying the growth-inhibitory effects of NOEY2, the expression of cell-cycle-related proteins in the xenografts was evaluated. The expression of Ki67, cyclin D1, and CDK4, which is associated with the cell-cycle transition from the G1 to S phase, was diminished notably, whereas p53 protein level was markedly increased in the NOEY2 group (Fig. 1D). To address whether NOEY2 induces apoptotic cell death, we also performed western blotting to evaluate the expression of a major protease controlling apoptosis. The expression of cell death-related proteins, such as caspase-3, was significantly enhanced in the NOEY2-overexpressing tumours versus the controls (Fig. 1D). These results indicate that NOEY2 could reduce the tumour growth by activating apoptotic cell death *in vivo*. Accordingly, the expression of Bax was enhanced in the NOEY2-overexpressing group versus the controls. In contrast, the expression of anti-apoptotic, oncogenic, and anti-proliferation markers, such as Bcl-2, survivin, cyclo-oxygenase, and X-linked inhibitor of apoptosis protein, was conspicuously reduced in NOEY2-overexpressing tumours (Fig. 1E). Collectively, these results indicate that NOEY2 plays a pivotal role in preventing ovarian tumour progression.

We also confirmed the anti-angiogenic effects of NOEY2 in the tumours by counting the number of blood vessels stained with an antibody against CD31, a typical marker of endothelial cells. A fourfold reduction in the number of CD31-positive blood vessels was found in the tumour sections from the NOEY2-overexpressing mice (Fig. 1F). Western blotting results also demonstrated that the expression of VEGF and HIF-1α, and phosphorylation of VEGFR-2 (Tyr-1175) were markedly decreased in the NOEY2-overexpressing tumours versus the controls (Fig. 1G). Interestingly, the level of VEGFR-1 phosphorylation (Tyr-951) was not changed (Fig. 1G).

Finally, we assessed the effects of NOEY2 on the activation of PI3K since the pro-angiogenic effects of VEGF/VEGFR-2 are mediated by the PI3K/Akt signalling (Byrne *et al*., 2005). NOEY2 noticeably decreased the phosphorylation of PDK1, PI3K, Akt, mTOR, TSC-2, p70S6K, and GSK3β (Fig. 1H). These results strongly indicate that NOEY2 induces apoptotic cell death and suppresses tumour progression and the PI3K/Akt signalling pathway. In all, these data show that NOEY2 potently suppresses tumour growth and angiogenesis *in vivo*.

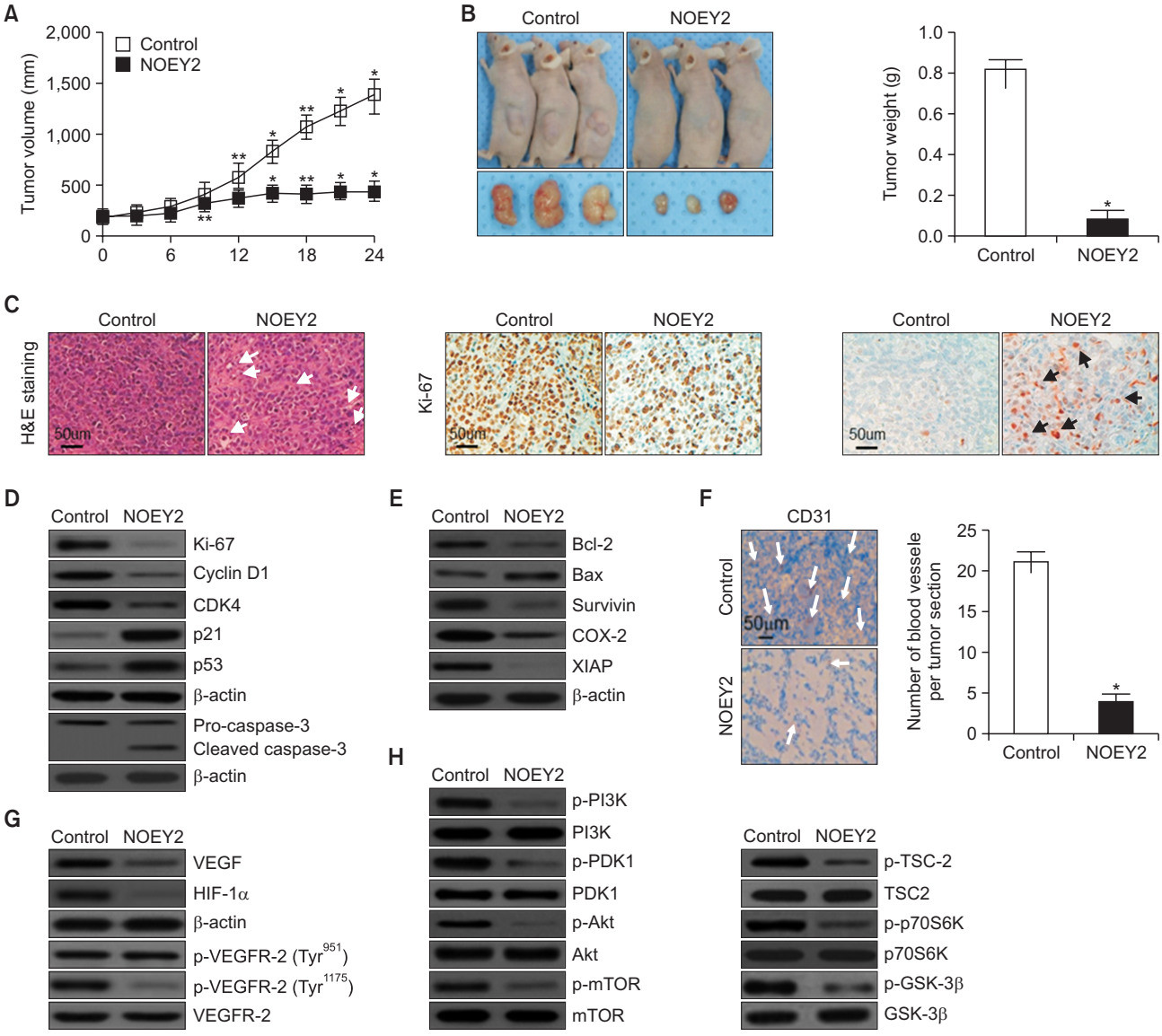

Fig. 1. NOEY2 inhibited tumour growth by suppressing angiogenesis *in vivo*. (A) Growth curves of human ovarian xenografts. NOEY2 stably transfected human SKOV-3 ovarian tumour cells, or empty vector (pcDNA3.1) stably transfected control cells were injected subcutaneously into nude mice to form tumours measuring 70 to 100 mm^3. Tumour size was calculated every 3 days. **p*<0.05; ***p*<0.01 versus control. (B) Tumours excised from control and NOEY2-overexpressed mice on day 28 of tumours measuring were photographed (left panel). Tumour weights were measured as the mean of three mice (n=5 per group) (right panel) ± SD. **p*<0.05 versus control. (C) Sections of NOEY2-overexpressed and control tumours were stained with H&E (left panel), cell proliferation markers Ki67 (middle panel), and cleaved caspase-3 (right panel) to observe cell morphology and apoptotic cell death (indicated with the arrows), respectively. Bars=50 μm. (D, E) Whole-protein extracts were isolated from tumours of xenografted mice and analysed by western blotting using indicated antibodies. β-actin was used to verify equal loading amounts among samples. (F) Endothelial cells in paraffin-embedded tumour sections were stained using anti-CD31 antibodies (left panel). Bar=50 μm. **p*<0.05 versus control. (G) Whole-protein extracts from tumours were evaluated the protein expression of VEGF, HIF-1α, phosphorylation of VEGFR-2 (Tyr-1175) and phosphorylation of VEGFR-2 (Tyr-951) by western blotting. β-actin and VEGFR-2 were used as the loading control. (H) Total cell lysates were prepared and detected by western blotting using anti-phospho-PI3K, anti-phospho-PDK1, anti-phospho-Akt, anti-phospho-mTOR, anti-phospho-TSC-2, anti-phospho-p70S6K and anti-phospho-GSK-3β antibodies. Total non-phosphorylated proteins (PI3K, PDK1, Akt, mTOR, TSC-2, p70S6K, and GSK-3β) were used to verify equal loading amounts among samples.

The N-terminal domain consisting of 34 amino acids (NOEY2-N) is necessary for NOEY2 (wild-type; wt)-mediated tumour growth suppression

NOEY2 can be divided into an N-terminal region unique to NOEY2, the main body having five conserved GTP binding sites, and the CAAX motif of the C-terminal region (Luo *et al*., 2003). In particular, the N-terminal region is unique for not existing in the RAS protein.

To identify the specific region responsible for the activity of anti-tumour effects, we generated three truncated NOEY2 ex-

pressing constructs (deletion of the GTP-binding, C-terminal, and N-terminal domains) (Fig. 2A, *top* panel).

To determine which regions of NOEY2 are important to induce cytotoxicity in SKOV-3 and OVCAR-3 ovarian cancer cells, the cells were transfected with the control (empty-vector only), NOEY2(wt), NOEY2 (ΔGTP BD), NOEY2 (ΔC-terminal), and NOEY2(ΔN-terminal), respectively. We first investigated the colony formation ability. The numbers of colonies formed were noticeably enhanced in NOEY2(ΔN-terminal)-only-transfected SKOV-3 and OVCAR-3 cancer cells, whereas two constructs, including NOEY2(wt), inhibited the colony formation (Fig. 2A, *bottom* panel).

Flow cytometric detection was then performed using labelled annexin V (Fig. 2B). The cells transfected with NOEY2(ΔN-terminal) showed no change in the early-stage or late-stage apoptotic fraction, as in the control. These observations suggest that cell growth suppression by NOEY2 results from increased apoptotic cell death and the N-terminus of NOEY2 (NOEY2-N) is essential to induce apoptosis. We next assessed the effects of NOEY2-N on cell viability by using the CellTiter-Glo assay kit as described in the methodology. As seen in Fig. 2C, the viability of the ovarian cancer cells was gradually diminished by treatment with NOEY2-N in a concentration-dependent manner. Subsequently, we examined whether this effect of NOEY2-N is related to the activation of caspase-3. NOEY2-N induced caspase-3 activity as much as NOEY2(wt) and significantly more than the control (Fig. 2D).

Since cleaved caspase-3 can induce the degradation of pro-PARP, we investigated whether the activation of caspase-3 induced by NOEY2(wt) or NOEY2-N ultimately induces the cleavage of pro-PARP. As shown in Fig. 2E, NOEY2-N induced the degradation of Pro-PARP as much as NOEY2(wt) (Fig. 2E).

Collectively, these results indicate that the N-terminal domain consisting of 34 amino acids might contribute to the apoptotic and anti-proliferative effects of NOEY2 in ovarian cancer cells.

NOEY2-N binds to VEGFR-2 but not VEGFR-1 and attenuates VEGF-induced VEGFR-2 phosphorylation (Tyr-1175)

NOEY2 inhibits tumour angiogenesis. We investigated whether NOEY2-N, which mimics the apoptotic effects of NOEY2, can also mimic the anti-angiogenic effect of NOEY2 on tumours. We first assessed the intracellular binding of NOEY2-N to VEGFR-1 and VEGFR-2. As presented in Fig. 3A, β-galactosidase was fully activated (92.19 ± 0.91) upon the interaction of NOEY2-N with VEGFR-2 but not with the empty vector (vector only: 1.92 ± 0.69) or VEGFR-1 (2.01 ± 0.72) (Fig. 3A). Therefore, in subsequent experiments, VEGFR-1 was used as a negative control. We next employed co-immunoprecipitation to confirm the direct interaction between NOEY2-N and VEGFR-2. DNA constructs expressing *NOEY2-N* (pcDNA3.1/Flag-NOEY2-N) and *VEGFR-1* (pcDNA3.1-VEGFR-1) or *VEGFR-2* (pcDNA3.1-VEGFR-2) or pcDNA3.1/Flag-NOEY2-N and vector only (pcDNA3.1) were co-transfected into HEK293T cells. Immunoprecipitation was then performed using an anti-Flag antibody and lysates from the transfected cells, and the precipitates were detected using an anti-NOEY2, anti-VEGFR-1, or anti- VEGFR-2 antibody. As shown in Fig. 3B, pcDNA3.1-VEGFR-2 co-immunoprecipitated with pcDNA3.1/Flag-NOEY2-N (*lane* 3 in the right panel), but not with VEGFR-1 (*lane* 3 in the left panel) or pcDNA3.1 (empty vector only) (*lane* 2 in the left panel) (Fig. 3B). VEGFR-2 is one of the key mediators of VEGF-induced endothelial cell function. Therefore, the inhibitory effect of NOEY2-N on VEGF-induced VEGFR-2 phosphorylation was evaluated in ovarian cancer cells *in vitro*. Ectopic expression of NOEY2-N remarkably suppressed the VEGF-induced VEGFR-2 phosphorylation (Tyr-1175) relative to that in the controls (Fig. 3C). In contrast, VEGFR-1 phosphorylation (Tyr-951) did not change (Fig. 3C). These data suggested that NOEY2-N inhibited VEGFR-2 phosphorylation in ovarian cancer cells *in vitro*. We examined the effects of NOEY2-N on the expression of VEGFR-2 in SKOV-3 and HUVECs by using the luciferase reporter assay, which used the VEGFR-2 promoter inserted upstream of the luciferase gene. The luciferase activity was gradually reduced in both cell lines by transient transfection of NOEY2-N in a dose-dependent manner (Fig. 3D). Next, we examined the effects of NOEY-N on the expression of VEGF and HIF-1α in SKOV-3 cells. As we expected, ectopic expression of NOEY2-N dramatically suppressed the expression of both VEGF and HIF-1α (Fig. 3E). In addition, the VEGF expression was gradually diminished by NOEY2-N in a concentration-dependent manner (Fig. 3F).

Collectively, we found that administration of NOEY2-N reduced the levels of VEGF, HIF-1α, and phosphorylation of VEGFR-2 (Tyr-1175) in ovarian cancer.

Construction of the three-dimensional structure of the human NOEY2 and identification of the potential key residues in the N-terminal domain

Homology-modelled structures for the main protein body and N-terminal domain of the human NOEY2 were firstly constructed using MODELER with four available template structures--three for the main protein body and one for the N-terminal domain (Fig. 4A-4C). Initially, the two separately constructed structures were manually connected for the next step (Fig. 4D). To generate many different starting conformers, the homology-modelled and manually connected structure was equilibrated for 50 ps at an abnormally high temperature (350K). The five selected conformers are shown with a starting structure (green coloured in Fig. 4C), and from them, the final five conformations were obtained. We compared the five structures with each other and found three structures with a relatively similar shape. One of these three structures was finally chosen as the native conformer. We selected the structure whose entire N-terminus interacted with the main protein-body regions (Fig. 4D). This final structure is the very first three-dimensional structure of the human NOEY2 protein.

To find or predict the key residues in the N-terminal domain, the selected final structure (Fig. 4D) was carefully investigated. Two different views of the final native structure (Fig. 4E, 4F) provide the relative position between the N-terminal domain and the main body. By checking the position of each residue in the N-terminal domain, residues 15 and 16 can easily be seen in the hinge region of the N-terminal domain. Therefore, Lys15 and Arg16 can be regarded as potential key residues in the N-terminal domain. Lys15 interacts with the side chains of the two main body residues through the backbone oxygen atom. The distances from the oxygen atom of Lys15, to NE2 of Gln189 and to CZ2 of Trp57 are 3.14 Å and 3.27 Å, respectively (Fig. 4G). Arg16 interacts with the main body in a very different way than Lys15 does. Arg16 uses the

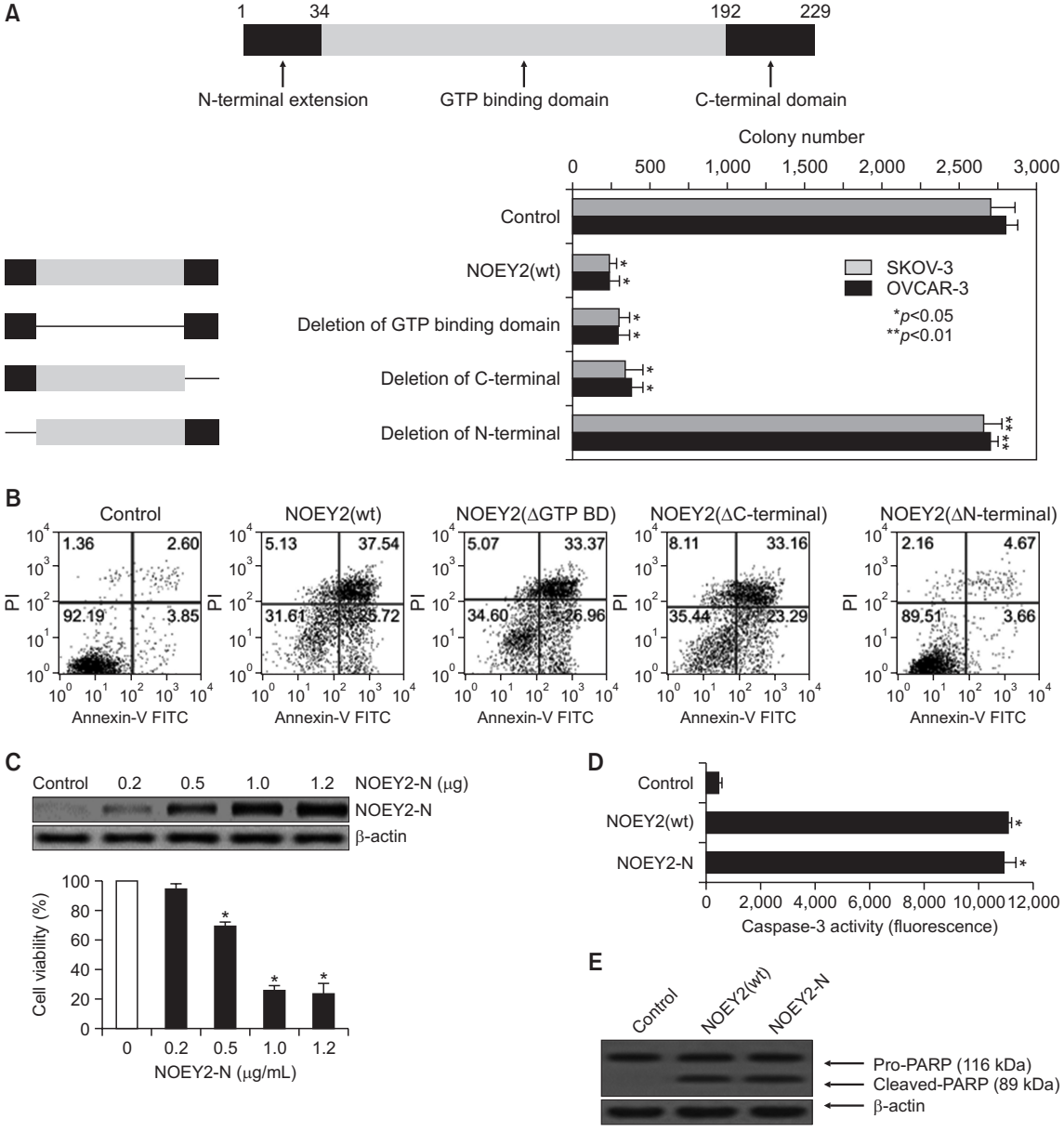

Fig. 2. N-terminal domain consisting of 34 amino acids is necessary for NOEY2(wt)-mediated tumour growth. (A) To assess the inhibitory effect, we generated three truncated NOEY2-expressing constructs (deletion of GTP-binding domain, deletion of C-terminal and deletion of N-terminal). Ovarian tumour cells were transfected with control (empty-inserted vector only), NOEY2(wt), NOEY2 (ΔGTP BD), NOEY2 (ΔC-terminal) or NOEY2(ΔN-terminal), respectively. Transfected cells were re-plated in 100-mm diameter dishes and grown for 14 days. Numbers of crystal violet-stained colonies were counted. Data are presented as mean ± SD from three independent experiments. *p<0.05; **p<0.01 compared to control. (B) Cell distribution of early-stage and late-stage apoptotic cell death was calculated using FACScalibur. Cells were maintained on 60 mm-diameter plates and transfected with control (empty-inserted expression vector only), NOEY2(wt), NOEY2 (ΔGTP BD), NOEY2 (ΔC-terminal) or NOEY2(ΔN-terminal), respectively. Cells were treated with FITC-labelled annexin V, propidium iodide. (C) Cell proliferation was evaluated using the CellTiter-Glo assay system. SKOV-3 cells were grown at a density of 4.5×10^3 per well in 96-well plates. After 24 h, cells were transfected with various concentrations of NOEY2-N. Each data point represents triplicate samples, and bars indicate mean ± SD. *p<0.05 versus zero concentration. (D) Caspase-3 activity was measured using a microplate reader in fluorescence mode with 400 nm (excitation wavelength) and 505 nm (emission wavelength). Enzyme activity was evaluated and indicated as fluorescence by the formula supplied by the manufacturer. The data shown represent three independent experiments. *p<0.05 compared to control. (E) PARP cleavage activated by control, NOEY2(wt) or NOEY2-N transfection. Soluble protein extracts were prepared and visualised by western blotting for cleaved PARP. Experiments were repeated at least three times with similar results. β-actin was used as a loading control.

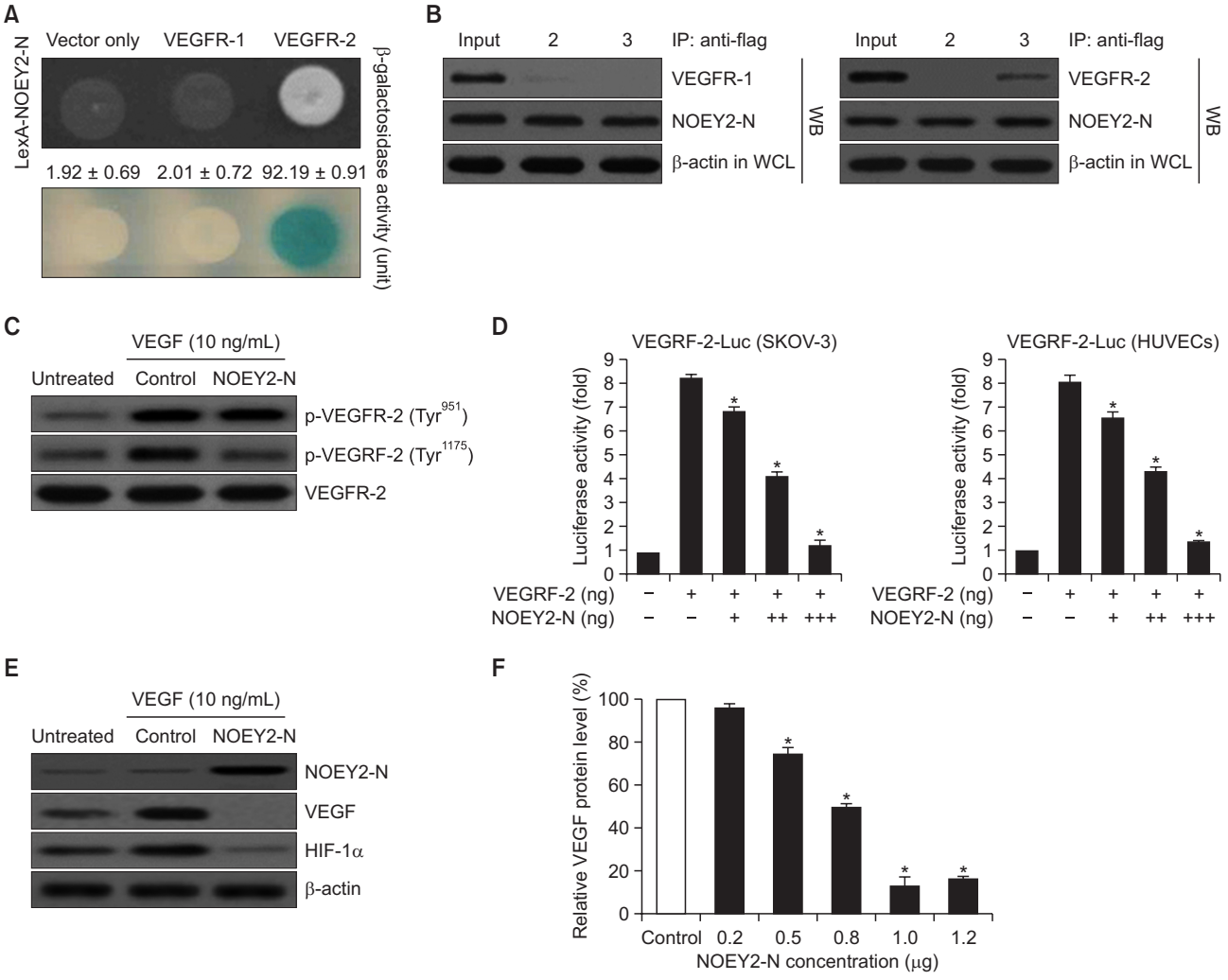

Fig. 3. NOEY2-N directly binds with VEGFR-2 but not VEGFR-1 and reduces VEGF-induced VEGFR-2 phosphorylation (Tyr-1175). (A) Positive interactions were validated by monitoring cell growth on a medium lacking leucine (upper panel) and forming blue colonies (lower panel) on X-gal plates, including 2% galactose. β-galactosidase activity (unit), evaluated by adding ONPG, is presented below the corresponding lanes. Data are presented as mean ± SD from three independent experiments. (B) Co-IP of NOEY2-N with VEGFR-1 or VEGFR-2. Immunoprecipitation (IP) was performed using anti-Flag antibodies in lysates from transfected HEK293T cells, followed by western blotting with anti-NOEY2, anti-VEGFR-1, and anti-VEGFR-2 antibodies. (Left panel) *lane* 2, pcDNA3.1 (expression vector only) and pcDNA3.1/Flag-NOEY2-N transfectant; *lane* 3, pcDNA3.1/Flag-NOEY2-N and pcDNA3.1-VEGFR-1 transfectant. (Right panel) *lane* 2, pcDNA3.1 (expression vector only) and pcDNA3.1/Flag-NOEY2-N transfectant; *lane* 3, pcDNA3.1/Flag-NOEY2-N and pcDNA3.1-VEGFR-2 transfectant. (C) SKOV-3 cells were treated with VEGF and then control-transfected or transfected with NOEY2-N. NOEY2-N significantly reduced phosphorylation of VEGFR-2 (Tyr-1175) triggered by VEGF. Phosphorylation of VEGFR-2 (Tyr-951 or Tyr-1175) was assessed by the specific antibody. VEGFR-2 was used as the loading control. (D) Inhibitory effect of VEGFR-2-dependent transcription by NOEY2-N. SKOV-3 and HUVECs were co-transfected with 500 ng of a VEGFR-2 expression plasmid (pcDNA3.1/VEGFR-2), 500 ng of VEGFR-2-Luc, and increasing concentrations of plasmid-encoding NOEY2-N (pcDNA3.1/Flag-NOEY2-N) (50, 250 and 500 ng). Data are presented as mean ± SD from three independent experiments. **p*<0.05 compared to control. (E) SKOV-3 cells were incubated with/without 10 ng/mL VEGF stimulator and were then control (expression vector only)-transfected or transfected with NOEY2-N. Expression levels of VEGF and HIF-1α were then visualised by immunoblotting. Experiments were repeated at least three times with similar results. (F) SKOV-3 cells were seeded to a confluence of 80%. Exponentially growing cells were transfected with increased concentrations of NOEY2-N (0.0-1.2 μg). Expression levels of VEGF were calculated by scanning densitometry and normalised to levels of loading control. Each data point represents triplicate samples, and bars indicate mean ± SD. **p*<0.05 compared to control.

side-chain atom, whereas Lys15 uses the backbone atom for the interaction. Additionally, Arg16 interacts with the backbone atoms from the main-body residues, whereas Lys15 interacts with the side-chain atoms from the main-body residues (Fig. 4H). For Arg16, the distance between the NH2 and oxygen of Gly79 is 2.80 Å, and the distance between NE and oxygen of His82 is also 2.80 Å (Fig. 4H).

The K15 and R16 residues are essential for apoptosis and angiogenesis

The mutants ^{15}KR^{16} of NOEY2-N by Ala, Asn, Asp, and Ser scanning mutagenesis were first determined by testing their

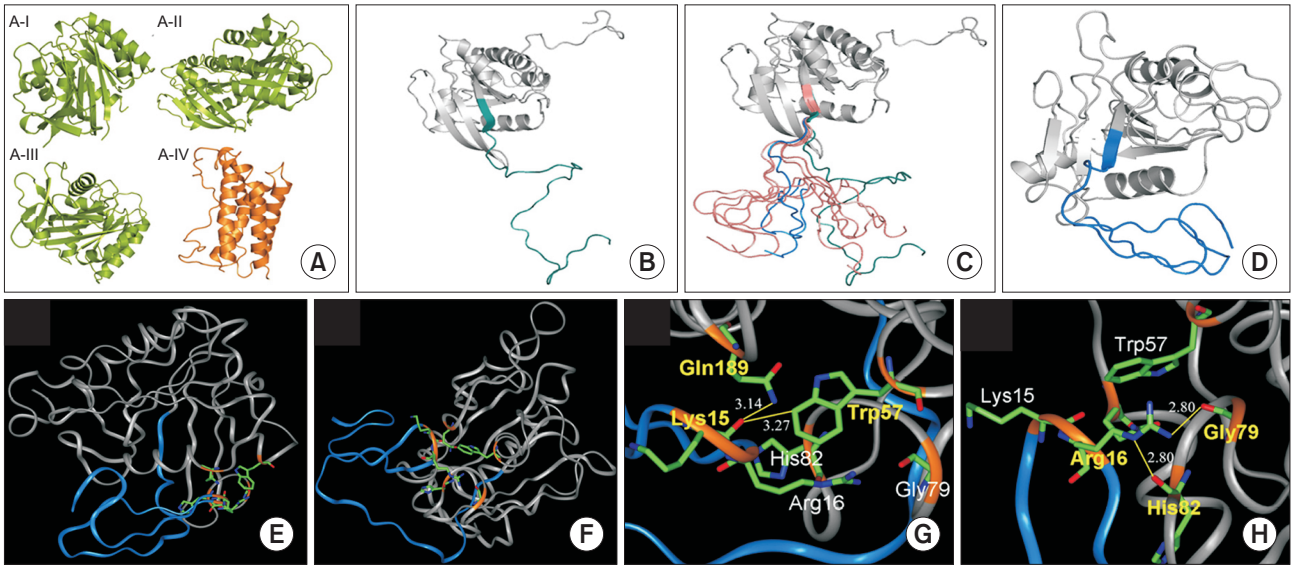

Fig. 4. Constructing three-dimensional structure of NOEY2 by homology modelling and prediction of the potential key residues in the N-terminal domain of human NOEY2. (A) Four x-ray and NMR structures were used as template structures for homology modelling of NOEY2. A-I, Rap1A (PDB code: 1GUA), A-II, Rap2A (3RAP), A-III, H-Ras (1K8R), A-IV, interleukin 6 (1IL6). In panel A, structures in green are used for the main body of the NOEY2 model, and the orange-coloured structure is a reference for the N-terminal domain. (B) Manually connected initial model of NOEY2. N-terminal domain is shown in cyan, with grey showing the main body. (C) Five different conformations of the N-termini domain were selected from a 50 ps equilibration run for the production run (in salmon colours). The starting structure is green; the blue-coloured N-terminal conformation in the Figure was used for further detailed analysis. (D) Final simulated structure for human NOEY2 protein. N-terminus and the main body of the protein are coloured blue and grey, respectively. This structure was time evolved from one of five conformers (blue colour in panel C). The Figure was generated with PYMOL (http://pymol.sourceforge.net). (E, F) Two different angle views of key residues in the ribbon diagram, main body and N-terminus domain, are shown in grey and blue colour, respectively. Key residues are highlighted as a stick model with element colours. (G) Interaction of backbone oxygen atoms in carboxyl group of Lys15 with the two side chains of Trp57 (3.27 Å) and Gln189 (3.14 Å). (H) Interaction of side chain Arg16 with the two backbone oxygen atoms of Gly79 (2.80 Å) and His82 (2.80 Å). Hydrogen bonds are shown as a yellow line. The backbone of the key residues highlighted in golden yellow. Atom colours in stick model: red – oxygen, blue – nitrogen, and green – carbon. INSIGHT II program (Accelrys, Inc., San Diego, CA, USA) was used to produce the Figures.

effects on the proliferation and death of endothelial cells. In general, VEGF enhanced the DNA synthesis of the un-transfected cells, and the cells transfected with the empty vector were comparable to non-induced cells (Plate *et al*., 1992). HUVECs were treated with each of the mutants, and cell proliferation was monitored by incorporating [^{3}H] thymidine. The N-termini of the NOEY2 mutants involved K15A, K15D, K15N, K15S, R16D, R16N and R16S, which suppressed cell proliferation to approximately 50-60% of that of the controls, whereas the R16A mutant did not have any effect (Fig. 5A). The N-termini of the NOEY2 mutants K15A, K15D, K15N, K15S, R16D, R16N, and R16S induced the apoptosis of SKOV-3 cells, whereas R16A again did not (Fig. 5B), as determined by observing apoptotic cell morphology (data not shown) and caspase-3 activity (Fig. 5C). Subsequently, to confirm the angiogenic effects of these various mutants, we conducted the capillary-like structure formation assay on Matrigel, an *in vitro* angiogenesis model, by using HUVECs.

As seen in Fig. 6A, the un-transfected or control cells incubated with VEGF formed a capillary-like tubule structure on Matrigel. In contrast, the K15A, K15A, K15D, K15N, K15S, R16D, R16N, and R16S mutants, including NOEY2-N (positive control), completely disrupted the VEGF-induced capillary-like tubular structure, but the R16A mutant did not (Fig. 6B). Finally, we examined the effects of the NOEY2 mutants on the expression of VEGF and HIF-1α by immunoblotting. As expected, the N-termini of the NOEY2 mutants, including K15A, K15D, K15N, K15S, R16D, R16N, and R16S, dramatically suppressed the expression of both VEGF and HIF-1α, whereas R16A did not (Fig. 6C).

Taken together, these results strongly suggest that the R16 residue within the N-terminal region is a key residue involved in the apoptotic and anti-angiogenic activities of NOEY2.

DISCUSSION

Currently, ovarian cancer remains the most fatal of the gynaecological malignant tumours in women worldwide, and its incidence increases every year (Sung *et al*., 2021). Typically, the prognosis is poor because ovarian cancer often metastasises early before it is diagnosed. Ovarian cancer metastases cannot grow to >1 mm without blood vessel formation and are thought to arise from epithelial cells in >90% of the cases. The endothelial cells of tumour vessels depend on pro-angiogenic components for proliferation and can proliferate more quickly than the vessels of healthy tissues, thus providing a target for anti-angiogenic therapy (Bamberger and Perrett, 2002; Conteduca *et al*., 2014). Generally, cytoreductive surgery and chemotherapy with platinum compounds are the suggested standard treatments for advanced ovarian cancer (Tuninetti *et al*., 2020). Unfortunately, more than half of patients with advanced

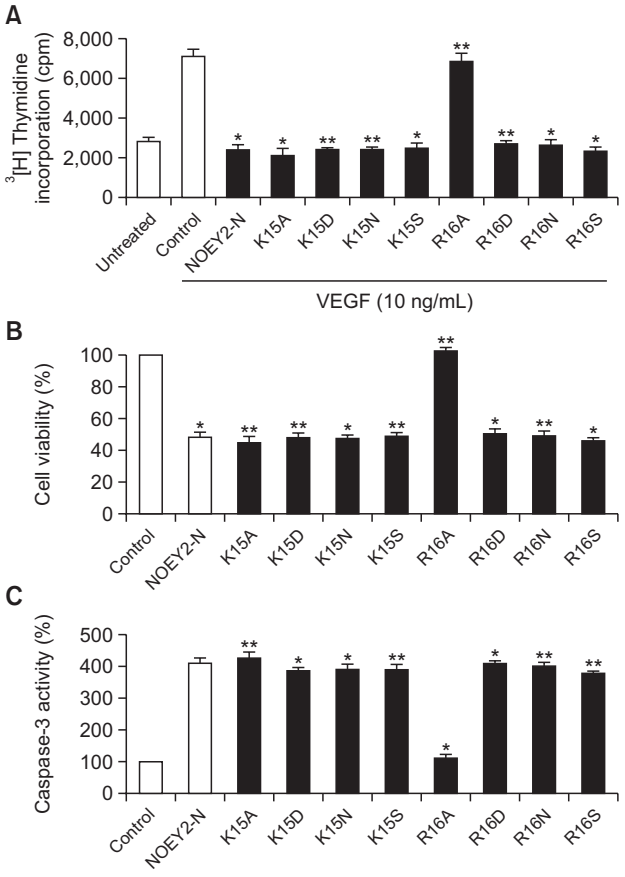

Fig. 5. NOEY2-N and eight mutants induce apoptosis via a caspase-3-dependent pathway. (A) The growth-inhibitory effect of NOEY2-N and eight mutants on endothelial cell proliferation. Cells were maintained and incubated for 3 days with/without VEGF. Counts per minute of [^{3}H] thymidine were calculated using a liquid scintillation counter. Each data point represents triplicate samples, and bars indicate mean ± SD. *p<0.05; **p<0.01 compared to control. (B) Cell proliferation was estimated using the CellTiter-Glo assay system. SKOV-3 cells were maintained at a density of 4.3×10^3 per well in 96-well plates. After 24 h, cells were transfected with NOEY2-N or various mutants. Data are presented as mean ± SD from three independent experiments. *p<0.05; **p<0.01 versus control. (C) Caspase-3 activity was estimated using a Spectramax 340 microplate reader (Molecular Devices, Sunnyvale, CA, USA) in fluorescence mode 400 nm (excitation) and 505 nm (emission) according to the manufacturer's instructions. Enzyme activity was evaluated from fluorescence values according to the formula provided by the manufacturer. Each data point represents triplicate samples, and bars indicate mean ± SD. *p<0.05; **p<0.01 compared to control.

ovarian cancer will eventually progress with recurrence and chemoresistance to platinum (Lheureux *et al*., 2019). Therefore, a new treatment strategy for ovarian cancer is urgently required.

NOEY2 is an imprinted tumour suppressor gene whose expression is lost or downregulated in ovarian and breast cancers; in this sense, this gene is different from the *Ras* oncogene. NOEY2 may be vital for tumour suppression. The VEGF-mediated Ras signal transduction in endothelial cells is also essential for angiogenic responses (Nishimoto *et al*., 2005). Over-expression of NOEY2 in mice results in reduced body size and impaired development in multiple organs. Bast *et al*. have reported that NOEY2 suppresses the STAT activity in breast and ovarian cancers, and lack of NOEY2 results in upregulation of the STAT activity, contributing to oncogenesis (Lu *et al*., 2008).

NOEY2 enhances autophagy by suppressing the Akt/mTOR-signalling pathway or by directly participating in the autophagy initiation complex through regulation of the nuclear localisation of the autophagy-associated transcription factor FOXO3 (Lu *et al*., 2014; Sutton *et al*., 2019). Zhong *et al*. (2019) have reported that NOEY2 downregulates the oncogenic Ras and induces autophagy via the Ras/Akt/mTOR pathway in glioblastoma. Recently, a novel mechanism of NOEY2-mediated inhibition of angiogenesis has been uncovered (Mao *et al*., 2019). NOEY2 is a new potent anti-angiogenic and anti-tumour protein that targets VEGF, HIF-1α, and p53. Here, we suggest a possible mechanism of NOEY2-mediated inhibition of angiogenesis and tumour growth. This mechanism, which involves direct binding of NOEY2 to VEGFR-2, whereby the PI3K-activated mTOR-signalling is inhibited.

In xenograft mouse models, tumour growth and angiogenesis are associated with HIF-1α expression. In addition, HIF-1α protein synthesis is controlled by promoting the PI3K/Akt and extracellular signal-regulated kinase (ERK)/MAPK-signalling pathways and is involved in tumour growth (Majmundar *et al*., 2010; Shi *et al*., 2021). Similar findings have been reported in studies on ovarian and brain cancers and indicated a regulatory role of HIF-1α in initiating angiogenesis via interactions with pro-angiogenic factors such as VEGF (Zagzag *et al*., 2000; Birner *et al*., 2001).

The over-expression of the tumour suppressor p53 under hypoxia may be linked to the HIF-1α-dependent pathway that initiates apoptosis. Furthermore, p53-independent pathways may provoke apoptotic cell death via the Bcl-2 pathway (Meadows *et al*., 2001). As shown in Fig. 1D, the levels of p53 protein and its transcriptional target p21 were markedly increased in NOEY2-transfected xenograft mice. However, the expression of the anti-apoptotic proteins Bcl-2 and Bcl-xL was strikingly decreased (Fig. 1E). Similarly, western blotting results demonstrated that the expression of VEGF and HIF-1α and the phosphorylation of VEGFR-2 (Tyr-1175) were markedly decreased in the NOEY2-treated tumours versus controls (Fig. 1G). In contrast, the level of VEGFR-2 phosphorylation (Tyr-951) did not change (Fig. 1G).

Finally, we used western blotting analysis to assess the expression of PI3K, a signalling factor downstream of VEGFR-2 in NOEY2-treated tumours. Treatment with NOEY2 noticeably decreased the phosphorylation, but not total levels, of PDK1, Akt, mTOR, TSC-2, p70S6K, and GSK-3β (Fig. 1H). These results strongly indicate that NOEY2 induces changes in the VEGFR-2 related PI3K/Akt signalling pathway.

Expression of VEGF has been proposed to be associated with the prognosis in ovarian cancer (Horikawa *et al*., 2017; Shen *et al*., 2017; Guo and Lu, 2018). VEGF exerts an angiogenic activity by directly interacting with VEGFR-2. The tumour suppressor NOEY2-N directly binds to VEGFR-2 but not VEGFR-1 (Fig. 3A, 3B). As shown in Fig. 3C, the ectopic expression of NOEY2-N diminished the VEGF-stimulated VEGFR-2 phosphorylation (Tyr-1175). In contrast, the VEGFR-2 phosphorylation of Tyr-951 was not suppressed. These results suggested that NOEY2-N mimics the anti-angiogenic effects of NOEY2.

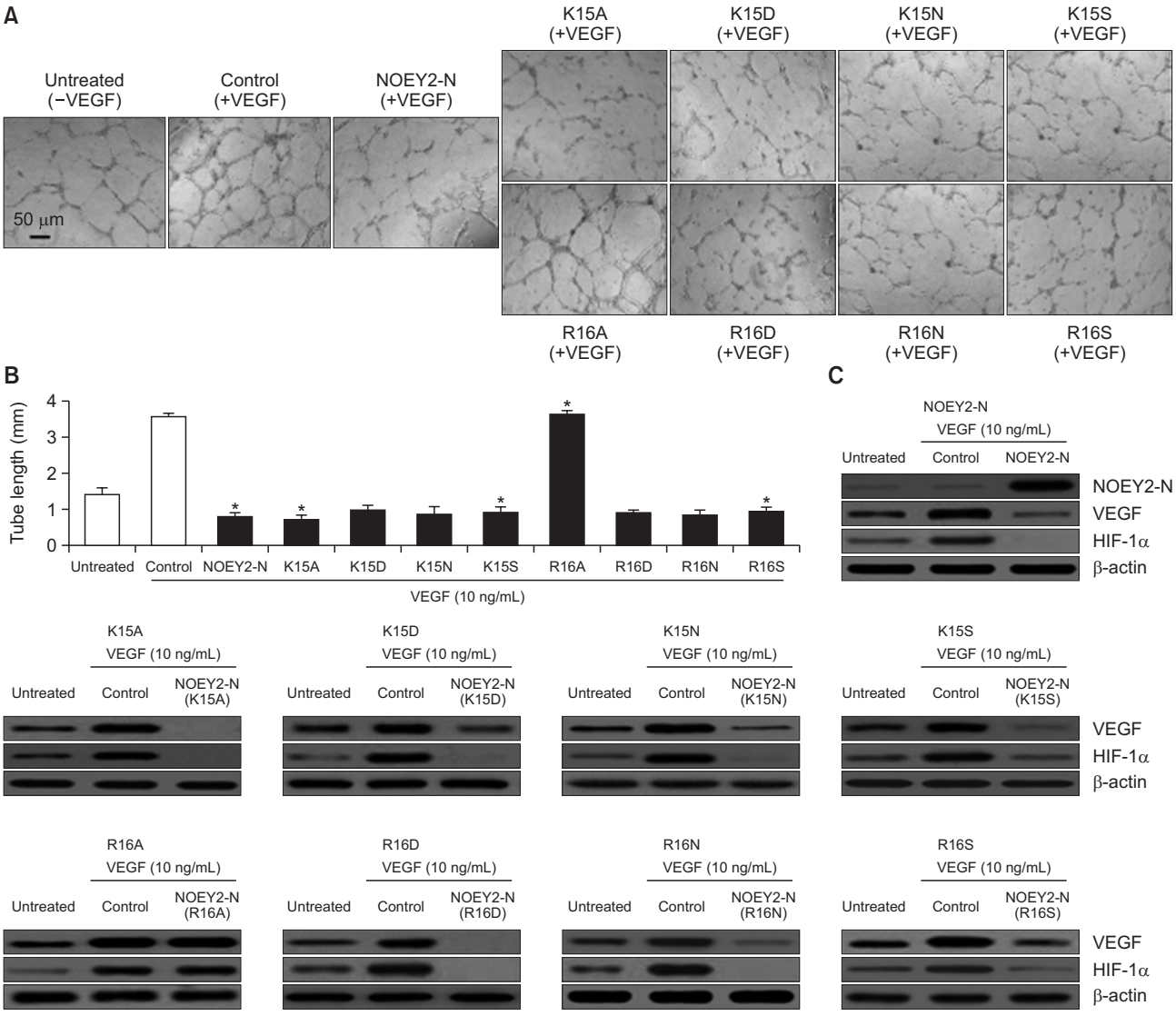

Fig. 6. The angiostatic activity of NOEY2-N and eight mutants of NOEY2-N. (A) After pre-treatment with/without VEGF, transfection with control, NOEY2-N, K15A, K15D, K15N, K15S, R16A, R16D, R16N, or R16S, respectively. Capillary-like tubule structures were imaged with a digital camera attached to an inverted microscope. Scale bars indicate 50 μm. (B) Quantitative evaluation of the angiostatic activity. Data presented as the mean length of tube formation in each sample. VEGF-treated expression vector only was used as a positive control. *p<0.05 versus control. Experiments were repeated three times with similar results. (C) SKOV-3 cells were incubated with/without 10 ng/mL VEGF stimulator and were then transfected with control, NOEY2-N or various mutants, respectively. Expression levels of VEGF and HIF-1α affect the proteins associated with angiogenesis control and therefore play vital roles in regulating tumour angiogenesis. Expression levels of VEGF and HIF-1α were visualised using western blotting. Experiments were repeated at least three times with similar results.

Through homology modelling of NOEY2, we predicted that K15 and R16, which reside in the hinge region of the N-terminal domain, are important for the intramolecular interaction with the main domain (Fig. 4). The importance of these two residues for the apoptosis and anti-angiogenic effects of NOEY2-N was evaluated through site-directed mutagenesis (Fig. 5, 6). We found that the R16 residue of NOEY2-N is important for the apoptotic and anti-angiogenic effects.

It has been reported that NOEY2-N can inhibit the RAS/MAPK signalling by directly binding to K-ras and H-ras (Sutton *et al*., 2019). These observations suggest the possibility that NOEY2-N may act as a RAS inhibitor. Our findings, which NOEY2-N directly binds to VEGFR2 and inhibits the downstream signalling, confirm and expand the importance and usefulness of NOEY2-N.

In summary, we propose that NOEY2 may overcome the deficiencies of the existing therapies that target VEGF, HIF-1α, p53, or the associated signalling pathways. With over-expression of NOEY2-N and its binding with VEGFR-2, it was observed that VEGF-induced endothelial cell was significantly diminished via inhibition of the VEGFR-2/mTOR/HIF-1α signalling pathway. NOEY2-N can have a greater inhibitory effect on tumour cells and tumour vessels with over-activated VEGF and HIF-1α signalling pathways. In particular, the R16 residue within the N-terminal region of NOEY2 is involved in the activation of apoptosis. The interaction of NOEY2-N with VEGFR-2

offers a useful mechanism for inhibiting oncogenesis. Further research on NOEY2-N and its tumour-suppressing characteristics may lead to effective anticancer therapies in the future.

CONFLICT OF INTEREST

The authors have declared that no competing interest exists.

ACKNOWLEDGMENTS

This study was partially supported by a grant from the National Cancer Center (NCC-0810410-3), BK21 FOUR program, the Basic Science Research Program, through the National Research Foundation (NRF) of Korea (NRF-2020R1A2C3004973, NRF-2018R1A5A2023127, NRF-2020M3E5E2038356), and Global PhD. Fellowship through the NRF of Korea (NRF-2018H1A2A1061990).

REFERENCES

Bamberger, E. S. and Perrett, C. W. (2002) Angiogenesis in epithelian ovarian cancer. *Mol. Pathol.* **55**, 348-359.

Bao, J. J., Le, X. F., Wang, R. Y., Yuan, J., Wang, L., Atkinson, E. N., LaPushin, R., Andreeff, M., Fang, B., Yu, Y. and Bast, R. C., Jr. (2002) Reexpression of the tumor suppressor gene ARHI induces apoptosis in ovarian and breast cancer cells through a caspase-independent calpain-dependent pathway. *Cancer Res.* **62**, 7264-7272.

Birner, P., Schindl, M., Obermair, A., Breitenecker, G. and Oberhuber, G. (2001) Expression of hypoxia-inducible factor 1alpha in epithelial ovarian tumors: its impact on prognosis and on response to chemotherapy. *Clin. Cancer Res.* **7**, 1661-1668.

Byrne, A. M., Bouchier-Hayes, D. J. and Harmey, J. H. (2005) Angiogenic and cell survival functions of vascular endothelial growth factor (VEGF). *J. Cell. Mol. Med.* **9**, 777-794.

Conteduca, V., Kopf, B., Burgio, S. L., Bianchi, E., Amadori, D. and De Giorgi, U. (2014) The emerging role of anti-angiogenic therapy in ovarian cancer (review). *Int. J. Oncol.* **44**, 1417-1424.

Dauber-Osguthorpe, P., Roberts, V. A., Osguthorpe, D. J., Wolff, J., Genest, M. and Hagler, A. T. (1988) Structure and energetics of ligand binding to proteins: Escherichia coli dihydrofolate reductase-trimethoprim, a drug-receptor system. *Proteins* **4**, 31-47.

Ferrara, N. (2002) VEGF and the quest for tumour angiogenesis factors. *Nat. Rev. Cancer* **2**, 795-803.

Gasper, R., Sot, B. and Wittinghofer, A. (2010) GTPase activity of Di-Ras proteins is stimulated by Rap1GAP proteins. *Small GTPases* **1**, 133-141.

Guo, B. Q. and Lu, W. Q. (2018) The prognostic significance of high/positive expression of tissue VEGF in ovarian cancer. *Oncotarget* **9**, 30552-30560.

Hicklin, D. J. and Ellis, L. M. (2005) Role of the vascular endothelial growth factor pathway in tumor growth and angiogenesis. *J. Clin. Oncol.* **23**, 1011-1027.

Horikawa, N., Abiko, K., Matsumura, N., Hamanishi, J., Baba, T., Yamaguchi, K., Yoshioka, Y., Koshiyama, M. and Konishi, I. (2017) Expression of vascular endothelial growth factor in ovarian cancer inhibits tumor immunity through the accumulation of myeloid-derived suppressor cells. *Clin. Cancer Res.* **23**, 587-599.

Jing, X., Yang, F., Shao, C., Wei, K., Xie, M., Shen, H. and Shu, Y. (2019) Role of hypoxia in cancer therapy by regulating the tumor microenvironment. *Mol. Cancer* **18**, 157.

Kang, S., Dong, S. M., Kim, B. R., Park, M. S., Trink, B., Byun, H. J. and Rho, S. B. (2012) Thioridazine induces apoptosis by targeting the PI3K/Akt/mTOR pathway in cervical and endometrial cancer cells. *Apoptosis* **17**, 989-997.

Kim, B. R., Seo, S. H., Park, M. S., Lee, S. H., Kwon, Y. and Rho, S. B. (2015) sMEK1 inhibits endothelial cell proliferation by attenuating VEGFR-2-dependent-Akt/eNOS/HIF-1alpha signaling pathways. *Oncotarget* **6**, 31830-31843.

Lheureux, S., Braunstein, M. and Oza, A. M. (2019) Epithelial ovarian cancer: Evolution of management in the era of precision medicine. *CA Cancer J. Clin.* **69**, 280-304.

Li, T., Kang, G., Wang, T. and Huang, H. (2018) Tumor angiogenesis and anti-angiogenic gene therapy for cancer. *Oncol. Lett.* **16**, 687-702.

Lu, Z., Luo, R. Z., Lu, Y., Zhang, X., Yu, Q., Khare, S., Kondo, S., Kondo, Y., Yu, Y., Mills, G. B., Liao, W. S. and Bast, R. C., Jr. (2008) The tumor suppressor gene ARHI regulates autophagy and tumor dormancy in human ovarian cancer cells. *J. Clin. Invest.* **118**, 3917-3929.

Lu, Z., Yang, H., Sutton, M. N., Yang, M., Clarke, C. H., Liao, W. S. and Bast, R. C., Jr. (2014) ARHI (DIRAS3) induces autophagy in ovarian cancer cells by downregulating the epidermal growth factor receptor, inhibiting PI3K and Ras/MAP signaling and activating the FOXo3a-mediated induction of Rab7. *Cell Death Differ.* **21**, 1275-1289.

Lugano, R., Ramachandran, M. and Dimberg, A. (2020) Tumor angiogenesis: causes, consequences, challenges and opportunities. *Cell. Mol. Life Sci.* **77**, 1745-1770.

Luo, R. Z., Fang, X., Marquez, R., Liu, S. Y., Mills, G. B., Liao, W. S., Yu, Y. and Bast, R. C. (2003) ARHI is a Ras-related small G-protein with a novel N-terminal extension that inhibits growth of ovarian and breast cancers. *Oncogene* **22**, 2897-2909.

Maharjan, S., Park, B. K., Lee, S. I., Lim, Y., Lee, K., Lee, Y. and Kwon, H. J. (2019) Gomisin G suppresses the growth of colon cancer cells by attenuation of AKT phosphorylation and arrest of cell cycle progression. *Biomol. Ther. (Seoul)* **27**, 210-215.

Majmundar, A. J., Wong, W. J. and Simon, M. C. (2010) Hypoxia-inducible factors and the response to hypoxic stress. *Mol. Cell* **40**, 294-309.

Mao, W., Peters, H. L., Sutton, M. N., Orozco, A. F., Pang, L., Yang, H., Lu, Z. and Bast, R. C., Jr. (2019) The role of vascular endothelial growth factor, interleukin 8, and insulinlike growth factor in sustaining autophagic DIRAS3-induced dormant ovarian cancer xenografts. *Cancer* **125**, 1267-1280.

Masoud, G. N. and Li, W. (2015) HIF-1alpha pathway: role, regulation and intervention for cancer therapy. *Acta Pharm. Sin. B* **5**, 378-389.

Meadows, K. N., Bryant, P. and Pumiglia, K. (2001) Vascular endothelial growth factor induction of the angiogenic phenotype requires Ras activation. *J. Biol. Chem.* **276**, 49289-49298.

Nishimoto, A., Yu, Y., Lu, Z., Mao, X., Ren, Z., Watowich, S. S., Mills, G. B., Liao, W. S., Chen, X., Bast, R. C., Jr. and Luo, R. Z. (2005) A Ras homologue member I directly inhibits signal transducers and activators of transcription 3 translocation and activity in human breast and ovarian cancer cells. *Cancer Res.* **65**, 6701-6710.

Plate, K. H., Breier, G., Weich, H. A. and Risau, W. (1992) Vascular endothelial growth factor is a potential tumour angiogenesis factor in human gliomas *in vivo*. *Nature* **359**, 845-848.

Rankin, E. B. and Giaccia, A. J. (2008) The role of hypoxia-inducible factors in tumorigenesis. *Cell Death Differ.* **15**, 678-685.

Rho, S. B., Kim, M. J., Lee, J. S., Seol, W., Motegi, H., Kim, S. and Shiba, K. (1999) Genetic dissection of protein-protein interactions in multi-tRNA synthetase complex. *Proc. Natl. Acad. Sci. U.S.A.* **96**, 4488-4493.

Rho, S. B., Lee, K. H., Kim, J. W., Shiba, K., Jo, Y. J. and Kim, S. (1996) Interaction between human tRNA synthetases involves repeated sequence elements. *Proc. Natl. Acad. Sci. U.S.A.* **93**, 10128-10133.

Rho, S. B., Lee, S. H., Byun, H. J., Kim, B. R. and Lee, C. H. (2020) IRF-1 inhibits angiogenic activity of HPV16 E6 oncoprotein in cervical cancer. *Int. J. Mol. Sci.* **21**, 7622.

Rho, S. B., Song, Y. J., Lim, M. C., Lee, S. H., Kim, B. R. and Park, S. Y. (2012) Programmed cell death 6 (PDCD6) inhibits angiogenesis through PI3K/mTOR/p70S6K pathway by interacting of VEGFR-2. *Cell. Signal.* **24**, 131-139.

Risau, W. (1997) Mechanisms of angiogenesis. *Nature* **386**, 671-674.

Shen, W., Li, H., Liu, L. and Cheng, J. (2017) Expression levels of PTEN, HIF-1alpha, and VEGF as prognostic factors in ovarian cancer. *Eur. Rev. Med. Pharmacol. Sci.* **21**, 2596-2603.

Shi, R., Liao, C. and Zhang, Q. (2021) Hypoxia-driven effects in cancer: characterization, mechanisms, and therapeutic implications. *Cells* **10**, 678.

Spannuth, W. A., Nick, A. M., Jennings, N. B., Armaiz-Pena, G. N., Mangala, L. S., Danes, C. G., Lin, Y. G., Merritt, W. M., Thaker, P. H., Kamat, A. A., Han, L. Y., Tonra, J. R., Coleman, R. L., Ellis, L. M. and Sood, A. K. (2009) Functional significance of VEGFR-2 on ovarian cancer cells. *Int. J. Cancer* **124**, 1045-1053.

Sung, H., Ferlay, J., Siegel, R. L., Laversanne, M., Soerjomataram, I., Jemal, A. and Bray, F. (2021) Global cancer statistics 2020: GLOBOCAN estimates of incidence and mortality worldwide for 36 cancers in 185 countries. *CA Cancer J. Clin.* **71**, 209-249.

Sutton, M. N., Lu, Z., Li, Y. C., Zhou, Y., Huang, T., Reger, A. S., Hurwitz, A. M., Palzkill, T., Logsdon, C., Liang, X., Gray, J. W., Nan, X., Hancock, J., Wahl, G. M. and Bast, R. C., Jr. (2019) DIRAS3 (ARHI) blocks RAS/MAPK signaling by binding directly to RAS and disrupting RAS clusters. *Cell Rep.* **29**, 3448-3459.e6.

Tuninetti, V., Di Napoli, M., Ghisoni, E., Maggiorotto, F., Robella, M., Scotto, G., Giannone, G., Turinetto, M., Siatis, D., Ponzone, R., Vaira, M., De Simone, M., Scaffa, C., Pignata, S., Greggi, S., Di Maio, M. and Valabrega, G. (2020) cytoreductive surgery for heavily pre-treated, platinum-resistant epithelial ovarian carcinoma: a two-center retrospective experience. *Cancers (Basel)* **12**, 2239.

Wang, X., Bove, A. M., Simone, G. and Ma, B. (2020) Molecular bases of VEGFR-2-mediated physiological function and pathological role. *Front. Cell Dev. Biol.* **8**, 599281.

Wigerup, C., Pahlman, S. and Bexell, D. (2016) Therapeutic targeting of hypoxia and hypoxia-inducible factors in cancer. *Pharmacol. Ther.* **164**, 152-169.

Yu, L., Kim, H. J., Park, M. K., Byun, H. J., Kim, E. J., Kim, B., Nguyen, M. T., Kim, J. H., Kang, G. J., Lee, H., Kim, S. Y., Rho, S. B. and Lee, C. H. (2021) Ethacrynic acid, a loop diuretic, suppresses epithelial-mesenchymal transition of A549 lung cancer cells via blocking of NDP-induced WNT signaling. *Biochem. Pharmacol.* **183**, 114339.

Yu, Y., Xu, F., Peng, H., Fang, X., Zhao, S., Li, Y., Cuevas, B., Kuo, W. L., Gray, J. W., Siciliano, M., Mills, G. B. and Bast, R. C., Jr. (1999) NOEY2 (ARHI), an imprinted putative tumor suppressor gene in ovarian and breast carcinomas. *Proc. Natl. Acad. Sci. U.S.A.* **96**, 214-219.

Zagzag, D., Zhong, H., Scalzitti, J. M., Laughner, E., Simons, J. W. and Semenza, G. L. (2000) Expression of hypoxia-inducible factor 1alpha in brain tumors: association with angiogenesis, invasion, and progression. *Cancer* **88**, 2606-2618.

Zhong, C., Shu, M., Ye, J., Wang, X., Chen, X., Liu, Z., Zhao, W., Zhao, B., Zheng, Z., Yin, Z., Gao, M., Zhao, H., Wang, K. and Zhao, S. (2019) Oncogenic Ras is downregulated by ARHI and induces autophagy by Ras/AKT/mTOR pathway in glioblastoma. *BMC Cancer* **19**, 441.